NAWI Graz
Natural Sciences

TU Graz

Alexander Julian Pfleger, BSc BSc

Dynamic Simulation of a Solid Oxide Fuel Cell System

MASTER'S THESIS

to achieve the university degree of

Diplom-Ingenieur

Master's degree programme: Technical Physics

submitted to

Graz University of Technology

Supervisor

Ao.Univ.-Prof. Dipl-Ing. Dr.techn. Gernot Pottlacher

Institute of Experimental Physics

in cooperation with AVL List GmbH

Graz, March 2021

AFFIDAVIT

I declare that I have authored this thesis independently, that I have not used other than the declared sources/resources, and that I have explicitly indicated all material which has been quoted either literally or by content from the sources used. The text document uploaded to TUGRAZonline is identical to the present master's thesis.

Abstract

The need for efficient and sustainable energy generation has grown during the last decades. Fuel cells have been proposed as a possible solution to this problem frequently. Still, fuel cells did not flood the market as one may expect. The conventional fuel cell has some drawbacks like moderate efficiency, high-cost catalysts, and low fuel-versatility. The modified fuel cell in the form of a solid oxide fuel cell (SOFC) operates at much higher temperatures, which helps to avoid the issues above.

Simulations are needed to prevent damage to the prototypes. Furthermore, simulations help to find efficient operation points and save costly testing time.

A 5 kW SOFC system located at AVL Graz, Austria, is scrutinized for this work. The partially existing SIMULINK model is expanded by a fuel side (anode path). The focus lies on connecting all modules with a continuous property vector, which contains gas composition, temperature, and pressure.

One of the main points is the implementation of the reforming reactions, taking place in the pre-reformer and the stack. For higher carbon-oxy-hydrates, a 0-dimensional approach is chosen. This new approach can reflect the reaction kinetics to a certain degree.

A second issue that was tackled is the efficient simulation of fuel recycling. A stable real-time solution is presented for the system used. This solution relies on the measured pressure difference of an added venturi tube.

Third, the literature values of thermodynamical data are reviewed. Depending on the source, some deviations occur. It is discussed if the implementation of a new dataset is desired and what problems may occur.

Kurzfassung

Der Bedarf an effizienter und nachhaltiger Energieerzeugung ist in den letzten Jahrzehnten gewachsen. Brennstoffzellen werden häufig als eine mögliche Lösung für dieses Problem vorgeschlagen. Dennoch haben Brennstoffzellen einen geringeren Marktanteil als erwartet. Die konventionelle Brennstoffzelle hat einige Nachteile, wie einen mäßigen Wirkungsgrad, die Notwendigkeit von teuren Katalysatoren und eine geringe Brennstoffverfügbarkeit. Die modifizierte Brennstoffzelle in Form einer Solid Oxide Fuel Cell (SOFC) arbeitet bei viel höheren Temperaturen, was hilft, die oben genannten Probleme zu vermeiden.

Simulationen sind notwendig, um Schäden an den Prototypen zu vermeiden. Außerdem helfen Simulationen, effiziente Betriebspunkte zu finden und kostbare Testzeit zu sparen.

Ein $5\,\mathrm{kW}$ SOFC-System, der AVL Graz, Österreich, wird in dieser Arbeit untersucht. Das teilweise vorhandene SIMULINK-Modell wird um einen Brennstoffpfad (Anodenpfad) erweitert. Der Fokus liegt auf der Verknüpfung aller Module durch einen kontinuierlichen Zustandsvektor, der Gaszusammensetzung, Temperatur und Druck enthält.

Einer der Hauptpunkte ist die Implementierung der Reformierungsreaktionen, die im Pre-Reformer und im Stack ablaufen. Für höhere Kohlenstoff-Sauerstoff-Wasserstoff-Verbindungen wird ein 0-dimensionaler Ansatz gewählt. Dieser neue Ansatz kann die Reaktionskinetik bis zu einem gewissen Grad wiedergeben.

Ein zweites diskutiertes Problem ist die effiziente Simulation des Brennstoffrecyclings. Für das verwendete System wird eine stabile Echtzeitlösung vorgestellt. Diese Lösung stützt sich auf die gemessene Druckdifferenz eines hinzugefügten Venturi-Rohrs.

Drittens werden die Literaturwerte der thermodynamischen Daten überprüft. Je nach Quelle treten einige Abweichungen auf. Es wird diskutiert, ob die Implementierung eines neuen Datensatzes gewünscht ist und welche Probleme dabei auftreten können.

Acknowledgements

I would like to thank my supervisors Gernot Pottlacher (TUG) and Martin Hauth (AVL), as well as Nikolaus Soukup for their guidance throughout this project.

Contents

List of Figures

List of Tables

1 Introduction

In today's world, the generation and the transport of electrical energy are of high necessity. Increasingly important is the search for alternatives to huge fossil fed power plants. Solid oxide fuel cells (SOFCs) offer a possibility to generate large amounts of energy on-site. The on-site generation minimizes transportation losses. Also, the missing electricity grid opposes fewer problems. The on-site generation is advantageous for implementations in remote buildings, ships, servers, and many others.

The simulation of SOFC systems allows cheaper and faster testing. The limits of new designs can be explored nondestructively. Optimal operation strategies can be approached before building the system. In this work, the focus lies on modeling an existing system to find new operation strategies.

1.1 Aim of the Work

The main goal of this work is to enhance and extend a partially existing simulation model of an SOFC system. Particularly the fuel path has to be implemented. The fuel path starts with an evaporator for liquid fuels. The fuel passes a reforming unit that processes the fuel for the stack. Therefore, also the chemical kinetics should be modeled. In the end, a basic version of the stack has to be built to model the electrochemical conversion. Submodels of the existing simulation should be utilized and improved if necessary.

The model should also suffice some core parameters. Primarily, the model should perform faster than in real-time. Furthermore, existing test cases should be replicable. It is also desired to perform basic predictions with the model.

1.2 Overview over Work

First, in the theory section, the system used is explained. A more detailed insight on the fuel path and all contained components is given. Then the physical and chemical fundamentals of these components are condensed. Further additional theory for building models of the components is presented. To describe the starting point of the building process of the simulation model an overview of the parts of the existing simulation model is given. At the end of the theory section literature values for

thermochemical data are compared with each other and ways to utilize these data in the simulation are presented.

Second, in the experimental section, the previously presented theory pieces are combined. Models are built for single components. The single-component models are united to a larger model. Here the choice of multiple simulation parameters is justified. Also, simplifications are addressed.

Third, the results and discussion section follows. Here uncertainties and limits of the models are investigated. In this process, experimental data from system tests are used for calibration and validation. Furthermore, existing problems are addressed and possible approaches for future improvements are given.

2 Theory

2.1 SOFC-System

A fuel cell is a device used to generate electrical energy from chemical fuel. In general, some kind of fuel and an oxidant are separated by an electrolyte. One of the two substances is ionized and passes the electrolyte to react with the other substance. The ion flow generates a potential between both sides of the electrolyte. By connecting both sides with a load, the electrical energy can be utilized.

For the electrolyte, a nonporous metal oxide is used, therefore, the name of the cell. The metal oxide makes it possible to operate the fuel cell at high temperatures. Common operating temperatures are in the order of $900\,\text{K}$ to $1300\,\text{K}$. A commonly used material for the electrolyte is Yttria(Y_2O_3)-stabilized zirconia(ZrO_2) or short YSZ. The huge benefit of this material is the higher ionic conductivity at higher temperatures with a relatively low loss in electric conductivity [1, 2]. Another benefit is the unnecessity of a catalyst. Due to the high operating temperatures, the desired reaction processes take place spontaneously. The uncatalyzed reactions help to reduce the overall costs of the system since noble metals like platinum can be omitted.

The metal oxide electrolyte has a high mass compared to other electrolytes. Therefore, SOFC systems are usually designed for stationary applications. Still, it is possible to design systems for a wide variety of target powers. Today SOFC systems in the range of $10^2\,\text{W}$ to $10^6\,\text{W}$ are in use. There are some applications in the mobile sector for systems with $10^2\,\text{W}$ to $10^3\,\text{W}$. Those systems only take the place of an auxiliary power unit (APU). In this work, only a $5\,\text{kW}$ system is discussed.

2.1.1 System design

The system design itself differs between various manufacturers. Still, most of the components used are equivalent. The system presented in figure 2.1 is only one possible way of operating an SOFC. This system can be split into three paths. First the *air path* or *cathode path* (dashed line), second the *fuel path* or *anode path* (thick line) and last the *exhaust path* (thin line). The stack connects those three paths.

Primarily the anode path is considered in this work. Therefore only components in this path are discussed in detail. For the other components, just a short overview

is given to understand their function. A detailed explanation can be found in the preceding works by Forster [3] and Soukup [4].
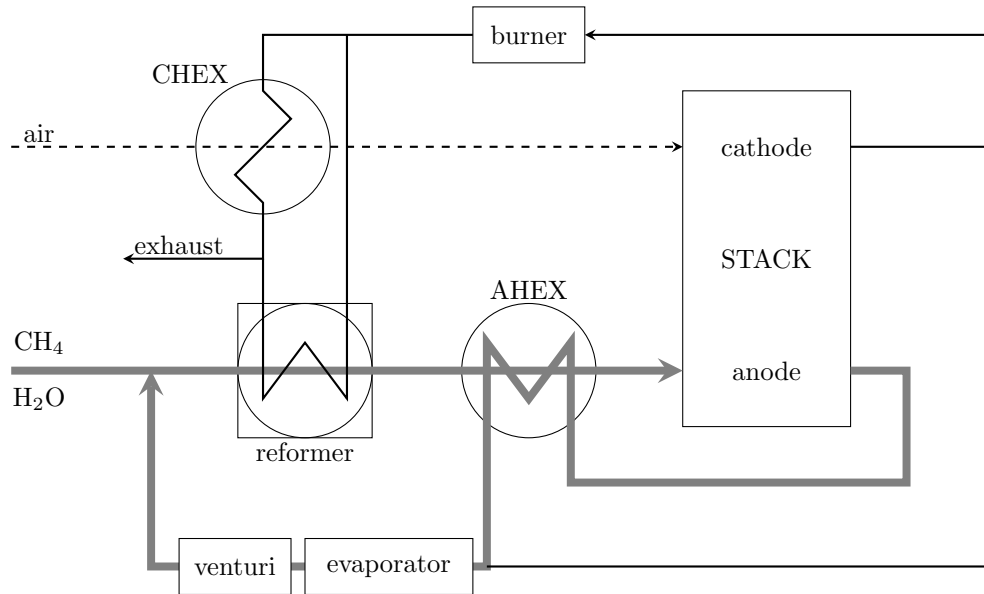
Figure 2.1: Process diagram for the SOFC system used. The thick line indicates the anode path. In this work, the anode path is looked upon primarily.

The cathode path provides oxygen for the fuel cell reactions. Oxygen is taken from the air. After entering the cathode path the air is preheated in the cathode heat exchanger (CHEX). Then it is transported directly to the stack. After leaving the stack it enters the exhaust path.

The anode path provides and processes the fuel for the cell. First the gaseous fuel and steam enter the anode path. Then the gas is forwarded to the reformer. The reformer is heated with a built-in heat exchanger (RHEX) and chemically converts the fuel into usable compounds for the cell. Usually, high amounts of Hydrogen are favored. The gas is preheated further with the anode heat exchanger (AHEX) before entering the stack. The gas stream at the end of the stack preheats the fuel in the AHEX. After passing the AHEX the stream is split in a manifold. One part is recycled and reenters the anode path. The other part enters the exhaust path.

The gas in the exhaust path may still contain fuel. Therefore, it passes a catalyst (CAT) to obtain fuel-free exhaust gases. This process heats the gas further and assists in maximizing energy utilization. The exhaust path is split into two separate streams. One delivers heat to the CHEX, the other to the RHEX. Later both streams are united and enter the exhaust system.

18

2.1.2 Stack

The stack is the core part of the system. All other components have only a supporting role. In the stack, electrical power is generated from chemical reactions directly. The stack consists of the anode and the cathode, which are separated by an electrolyte membrane. This membrane is permeable for particular ions only. The ion transfer between the electrodes generates an electrical potential. The resulting current is proportional to the ion current.

The stack is a very complex component of the simulation. It has to consider the mass transfer from cathode to anode. The mass transfer leads to chemical reactions on the anode side. These reactions contribute to the heat balance. Additionally, heat exchange between anode and cathode takes place. These factors affect the electric properties of the stack, which again affect the ion transfer.

2.1.3 Heat Exchanger

A heat exchanger (HEX) is a thermal connection between two hermetically separated regions in the system. It transports thermal energy from one point in the flow chart to another. A mass or pressure exchange does not take place. A simple implementation of a heat exchanger consists of two concentric pipes. Separate media are flowing through the pipes. For an ideal heat exchanger in the case of a parallel flow, the temperatures of both media will equalize after an infinite length. In case of an antiparallel flow, the temperatures will exchange. Real heat exchangers may have way more complex designs and cannot reach these ideal limits.

The system uses heat exchangers at four positions. Most of the heat exchangers are used to preheat an incoming gas with waste gases. The heat exchanger in the stack is of less importance for the operation of the system but is required in the simulation and may contradict the previously made propositions. Mass transport takes place when an electrical current flows. This mass transport has to be considered in the simulation.

2.1.4 Reformer

The reformer synthesizes hydrogen and lower carbon-oxy-hydrates from higher carbon-oxy-hydrates. The discussed reformer uses the idea of steam oxidation. High amounts of gaseous water support the chemical processes. To accelerate the processes a nickel catalyst is used. The reformer is combined with a heat exchanger. The waste heat from the cathode path is used to heat the reformer. The added heat is necessary to run the reactions efficiently since the process of steam oxidation is endothermic.

In literature, this setup is referred to as a pre-reformer frequently, since it is separated from the stack. As an alternative, the fuel could be synthesized in the stack directly. In the system used it was refrained from using reforming in the stack. The main targets of the pre-reformer were better utilization of waste heat, higher versatility in fuels used, protection of the stack from carbon deposition, and higher efficiencies in the stack. In this work, *reformer* always stands for the pre-reformer concept.

2.1.5 Junctions

The system uses junctions at different positions, mainly in the anode path. Unlike in the cathode path the anode path recycles most of its gas. To add new mass to the system a junction is needed. A junction is an inlet in the real system. In the simulation, it has to be considered carefully. The junction not only changes the composition of the mass flow. Usually, it also changes the temperature and alters the total energy of the system.

The junctions in the recycling path are used to insert steam and gaseous fuels like methane into the system. Also, forming-gas can be inserted to guarantee a controlled heat-up process or to scrutinize the thermodynamic properties of the system. Further, junctions are in the exhaust path before the burner and after the cathode heat exchanger and the reformer. These junctions will not be investigated in this work but could be simulated with the same models.

2.1.6 Evaporator

In general, the evaporator is a special case of the junction. The evaporator provides the possibility to use different kinds of fuels that may be liquid under normal conditions. There are several different ways to insert liquids into gases. In this system, a thermic evaporator is used. The liquid is put onto a metal mesh. Through capillary processes, the liquid moistens the whole mesh, providing a large surface. When hot gas flows over the mesh, the liquid evaporates, and the gas cools down. The liquid is preheated, to make this process more efficient. Otherwise, the gas may cool down too much. Using a purely thermic evaporator makes nozzles in the gas flow unnecessary that would generate a pressure loss. This way the system can also be used with gaseous fuels without major modifications to prevent large losses.

2.1.7 Interactions

In this thesis, one large circle of interactions is of importance. In the anode path reformer, AHEX, stack an evaporator form a loop. This loop is called the recycling path. It is fed by fuel and steam. Over the manifold, excess gas leaves the loop. A blower forces the circulation of the gas. All components in the loop affect the

gas properties and consequently, the splitting ratio at the manifold. A venturi tube inside the loop is used to determine the mass flow.

Furthermore, all components interact with each other with the driving force of an overall equilibrium in temperature. Some of these interactions are desired like in a heat exchanger. Other heat transfers occur due to the vicinity of components and pipes in the system design. Most of them are unwanted. These vicinities are not visible in the flow chart in fig. 2.1, but can be found by investigating a specific real system.

2.2 Reforming

Reforming is a process to convert higher carbon-oxy-hydrates to a gas containing lower carbon-oxy-hydrates and/or hydrogen. There are three major types: Autothermic reforming, partial oxidation, and steam reforming. In the next paragraphs, only steam reforming will be discussed, since it is the method used in the models. For further reading on the other methods [5], [6], [7], and [8] is recommended.

In the steam reforming process, carbon-oxy-hydrates react with steam in a catalyst. There are two major reactions to describe this process, the reforming reaction and the water-gas shift reaction.

In the reforming reaction carbon-oxy-hydrates react with steam to carbon monoxide and hydrogen, like shown in the equation

$$\text{C}_c\text{H}_h\text{O}_o + (c-o)\text{H}_2\text{O} \rightarrow c\text{CO} + (c-o+h/2)\text{H}_2 - \Delta H^0 \ . \tag{2.1}$$
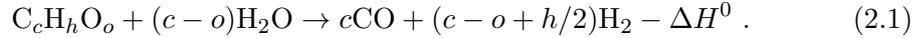
In this work methane or diesel are used for $\text{C}_c\text{H}_h\text{O}_o$. This reaction is endothermic because the reaction enthalpy ΔH^0 is negative [3]. For the case of methane ($c = 1, h = 4, o = 0$) this reaction is reversible and can be written as:

$$\text{CH}_4 + \text{H}_2\text{O} \rightleftharpoons \text{CO} + 3\text{H}_2 - \Delta H^0 \tag{2.2}$$

Together with the water-gas shift reaction the final equilibrium can be determined. The water-gas shift reaction describes the equilibrium of carbon monoxide, water, carbon dioxide, and hydrogen and can be written as:

$$\text{CO} + \text{H}_2\text{O} \rightleftharpoons \text{CO}_2 + \text{H}_2 \ . \tag{2.3}$$

For higher temperatures the equilibrium shifts to the left of (2.3) ($\text{CO} + \text{H}_2\text{O}$).

The stochastically required amount of steam can be calculated with (2.1). Putting the quantity of steam in relation to the total number of carbon atoms gives the steam carbon ratio SCR:

$$SCR = \frac{S}{C} = \frac{\dot{N}_{H_2O,in}}{\dot{N}_{C,in}} \ .$$

Theoretically, $SCR = 1$ is sufficient to convert all carbon-oxy-hydrates. Experiments have shown, the SCR depends on the temperature. If the SCR is too low there will be a carbon deposition in the reformer even at higher temperatures. This carbon deposition has to be avoided since it harms the system. An $SCR > 1$ is needed to accomplish this.

2.2.1 Equilibrium

The equilibrium for both reactions depends on temperature and pressure. For the reforming reaction, higher temperatures would lead to higher quantities of hydrogen and minor carbon deposition, the water-gas shift reaction favors lower temperatures, which leads to an optimum of $T \approx 1000\,\mathrm{K}$ with a pressure of $p = 10^5\,\mathrm{Pa}$ and $SCR = 1.5$. In figure 2.2 the resulting concentrations are plotted over different temperatures using only diesel and steam with $SCR = 1.5$. For low temperatures $(T < 870\,\mathrm{K})$ a significant carbon deposition takes place.
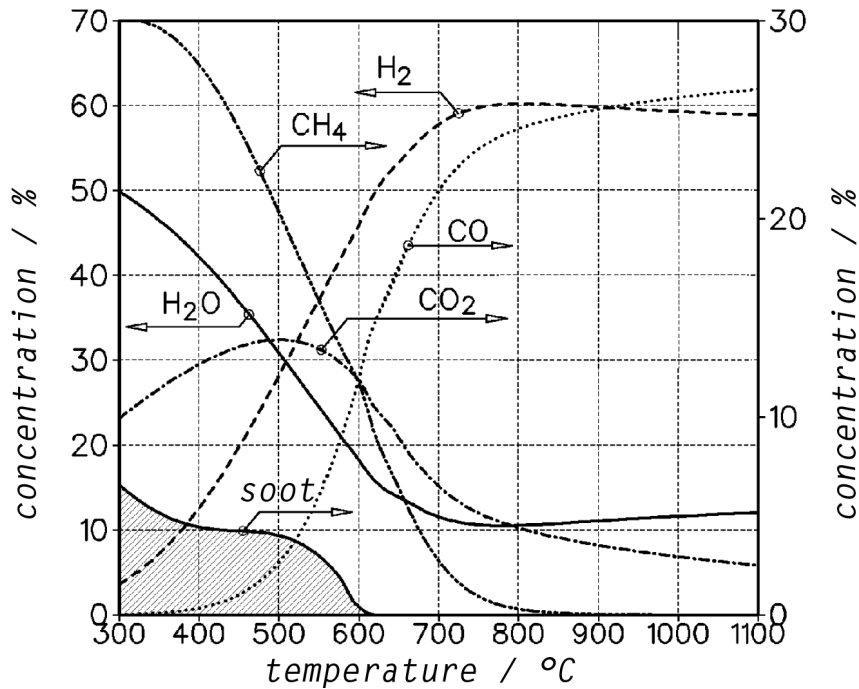

Figure 2.2: Temperature dependend gas composition for steam reformed diesel with $SCR = 1.5$ at $p = 10^5\,\mathrm{Pa}$. Adapted from [6].
The concentration shift from CH_4 and H_2O to CO and H_2 can be seen. At high temperatures less CO_2 can be expected. The grey area at low temperatures labeled *soot* marks the carbon deposition which has to be avoided.

There is already a reliable but slow MATLAB routine for the computation of the equilibrium state for a few carbon-oxy-hydrates. Yvonne Thaller converted this routine to a SIMULINK model, presented in [9]. The fundamental idea of the model is that the Gibbs enthalpy is minimized for the equilibrium state [10].

The theory of the MATLAB routine and the SIMULINK model is described in detail in [9]. Here only the most important steps are discussed to give a short overview. Starting with the molar standard Gibbs enthalpy $G_{mj}^0(T, p^0)$ of a gas compound j, at a certain temperature T and the standard pressure $p^0 = 10^5 \, \text{Pa}$, the molar Gibbs enthalpy of an arbitrary gas can be calculated as follows [9, 11] (values for $G_{mj}^0(T, p^0)$ can be found in tables):

$$G = \sum_j G_{mj}(T, p_j) = \sum_j G_{mj}^0(T, p^0) + R_m T \ln \frac{p_j}{p^0} \tag{2.4}$$

With the assumption of an ideal gas with the gas constant R_m, the partial pressures p_j can be written as [9, 11]

$$p_j = p \frac{N_j}{N} \ , \tag{2.5}$$

with molar amount of each substance N_j and total amount $N = \sum_j N_j$. Inserting (2.4) into (2.5) yields the following equation:

$$G = \sum_j G_{mj}^0(T, p^0) + R_m T \ln N_j - R_m T \ln N + R_m T \ln \frac{p}{p^0} \tag{2.6}$$

In the model used this expression is divided by $R_m T$ since only the minimum of G is needed. G is evaluated at a certain temperature T and pressure p. Furthermore, the quantity of each element, in this case C, H, and O is known. Therefore, it only depends on the molecular composition of the gas. This optimization problem can be solved with the method of Lagrange multipliers. This yields a system of nonlinear equations, which is solved using the Newton-Raphson Method. The system can now be written in the form $\mathbf{A}\vec{x} = \vec{c}$ with [9, 12]:

$$\mathbf{A} = \sum_{k=1}^{NS} N_k \begin{pmatrix} a_{1,k}a_{1,k} & \cdots & a_{1,k}a_{NE,k} & a_{1,k} \\ \vdots & a_{i,k}a_{j,k} & \vdots & \vdots \\ a_{NE,k}a_{1,k} & \cdots & a_{NE,k}a_{NE,k} & a_{NE,k} \\ a_{1,k} & \cdots & a_{NE,k} & 1 - \frac{N}{kN_k} \end{pmatrix} \tag{2.7a}$$

$$\vec{x} = \begin{pmatrix} \pi_1 \\ \vdots \\ \pi_{NE} \\ \Delta \ln N \end{pmatrix} \tag{2.7b}$$

23

$$\vec{c} = \begin{pmatrix} b_1^0 - b_1 \\ \vdots \\ b_{NE}^0 - b_{NE} \\ \dot{N} \end{pmatrix} + \sum_{k=1}^{NS} N_k \frac{G_{mk}}{R_m T} \begin{pmatrix} a_{1,k} \\ \vdots \\ a_{NE,k} \\ 1 - \frac{R_m T}{G_{mk}} \end{pmatrix} \tag{2.7c}$$

NS number of different species

NE number of different elements

$a_{i,k}$ number of atoms of element i in a molekule of species k

b_i^0 assigned kilogram-atoms of element i per kilogram reactant

b_i kilogram-atoms of element i per kilogram of mixture

$\pi_i, \Delta \ln N$ correction variables

With the Lagrange multipliers, a better solution can be calculated. This improved solution is used as a new starting point. The whole process is repeated, till the error towards the algebraic optimum is small enough. The model aborts the iterative search when the difference between two calculated solutions is below the desired limit (or of course the number of iterations reaches a limit).

2.2.2 Classical approach

In a real system, it takes time to get to the equilibrium state. Catalysts can speed the reaction up; still, there is no guarantee of reaching the equilibrium state, making the sole calculation of the equilibrium composition insufficient. A real system can be examined using chemical kinetics. Starting from a set of input parameters including temperature, pressure, flow speed, composition of the catalyst, and geometry of the system, the chemical processes can be described accurately.

The time dependence of an arbitrary reaction can be described using the concentration c_i of the reactant i and the reaction velocity c_i'. Those parameters can be put in relation with the following differential equation.

$$c_i' = k \prod_{j=1}^{n} c_j \tag{2.8}$$

where k is the specific reaction constant and n indicates the order of the reaction. The parameter k can be determined experimentally. The parameter n depends on the number of reactants, making the case $0 < n < 3$ common. The case $n = 0$ is used mainly for catalytic reactions. Solving (2.8) yields the favored time dependence $c_i(t)$. For $n = 1$ the dependence

$$c_i'(t) = c_i(0)e^{kt} \tag{2.9}$$

can be found. It is used to describe decaying processes. The solutions for reactions $n \neq 1$ are not used in this work, but can be deducted by solving (2.8) or consulting standard works.

Equation (2.9) depends on k which in reality itself depends on the temperature T. To obtain an universal equation the step $k = k(T)$ has to be done. This can be done using the Arrhenius law:

$$k(T) \propto e^{\frac{-a}{T}} \tag{2.10}$$

whereas a is a function of the activation energy of the reaction. The Arrhenius law is not precise but gives a good estimation. This strong dependence has to be considered when investigating reactions at different temperatures. A temperature difference $\Delta T = 10\,\mathrm{K}$ can already double the reaction speed in case of small activation energies like $E_a = 60\,\mathrm{kJ \cdot mol^{-1}}$. For higher activation energies the speed difference is also higher [13].

2.3 Venturi

Determining the correct mass flow in the anode path is difficult and imprecise by only analyzing the input and output streams of the whole system. To get information about the actual mass flow and the recycling rate, an in-situ measurement is inevitable. This measurement is done with the help of a Venturi tube. The Venturi tube is a tube divided into two connected segments with different cross-sections. A fluid or gas flowing through the Venturi tube has a different static pressure in both parts. With the resulting pressure difference Δp, it is possible to calculate the flow speed for a known fluid or gas.

The Bernoulli's Equation is taken to derive the pressure difference Δp and massflow $\dot{m} = \dot{m}(\Delta p)$:

$$\frac{v_i^2}{2} + \frac{p_i}{\rho} + gz_i = const. \tag{2.11}$$

where for the segment i of the tube v_i is the flowspeed, p_i the static pressure, g the gravitational acceleration, and z_i is the vertical position. ρ is the density of the fluid or gas used. Evaluating (2.11) at two different points of the tube obtains:

$$\frac{v_1^2}{2} + \frac{p_1}{\rho} + gz_1 = \frac{v_2^2}{2} + \frac{p_2}{\rho} + gz_2 \tag{2.12a}$$

$$\frac{p_1 - p_2}{\rho} + g(z_1 - z_2) = \frac{v_2^2 - v_1^2}{2} \tag{2.12b}$$

$$\underbrace{p_1 - p_2}_{\Delta p} + \rho g \underbrace{(z_1 - z_2)}_{\Delta z} = \frac{1}{2}\rho\left(v_2^2 - v_1^2\right) \tag{2.12c}$$

$$\Delta p + \rho g \Delta z = \frac{1}{2}\rho v_2^2 \left(1 - \frac{v_1^2}{v_2^2}\right) \tag{2.12d}$$

Using the mass conservation $v_i A_i = const.$ with the cross sections A_i (2.12) can be reshaped to:

$$\Delta p + \rho g \Delta z = \frac{1}{2}\rho v_2^2 \left(1 - \left(\frac{A_1}{A_2}\right)^2\right) \qquad (2.13a)$$

$$v_2 = \sqrt{\frac{2(\Delta p + \rho h \Delta z)}{\rho v_2^2 \left(1 - \left(\frac{A_1}{A_2}\right)^2\right)}} \qquad (2.13b)$$

The Venturi tube of the system has a horizontal position, thus $\Delta z = 0$ vanishes and the equation for the massflow can be obtained:

$$\dot{m}(\Delta p) = \rho A_2 v_2 = \frac{A_2}{\sqrt{1 - \left(\frac{A_1}{A_2}\right)^2}} \sqrt{2\rho}\sqrt{\Delta p} \qquad (2.14)$$

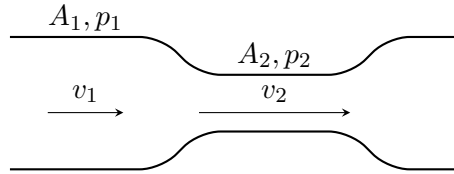In figure 2.3 a Venturi tube resembling this case is depicted.

Figure 2.3: Schematic of a horizontal Venturi tube. With the two different crosssections A_i. In the tube different flowspeeds v_i and static pressures p_i can be observed.

2.4 Junctions

The junction model is used to unite two or more gasses and to calculate the mixing temperature. Assuming there are no chemical reactions and phase transitions, the new mass flow $\dot{m}_{mix}$ can be obtained by summing the separate mass flows $\dot{m}_i$:

$$\dot{m}_{mix} = \sum_i m_i \qquad (2.15)$$

Using the energy conservation, the resulting temperature T_{mix} can be calculated by summing over the caloric energy flows $\dot{Q}_i$ for each incoming gas stream. Therefore, first the energy flows have to be determined using the specific heats c_i^p and the temperatures T_i of each stream. Second the total caloric energy of the new gas stream is divided by the heat capacity of the new gas stream:

$$\dot{Q}_i = \dot{m}_i T_i c_i^p \qquad (2.16)$$

$$T_{mix} = \frac{\sum_i \dot{Q}_i}{\sum_i \dot{m}_i c_i^p} \tag{2.17}$$

Real gases have a temperature dependent heat capacity. Therefore, we have to set $c_i^p = c_i^p(T)$. In this case (2.17) gives a variance on the real value depending on the temperature differences of the initial gases. To obtain an accurate result the following integral has to be evaluated:

$$\sum_i \dot{Q}_i = \int_0^{T_{mix}} \sum_i \dot{m}_i c_i^p(T) dT \tag{2.18}$$
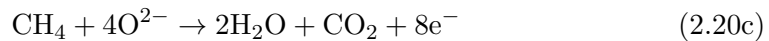
2.5 Stack

There are different ways to build a stack, including parameters like geometry and composition. In this section, only the YSZ-stack used is considered. Yet the theory used may apply to many other stack designs with slight modifications. After starting with the general structure, the chemical aspects and the occurring reactions are discussed. Then the electric properties and cell losses are explained. In the end, the efficiency of the stack is looked upon.

2.5.1 Reactions

On the cathode side of the stack only one reaction takes place. Molecular oxygen O_2 is cracked to atomic oxygen and ionized:

$$O_2 + 4e^- \rightarrow 2O^{2-} \tag{2.19}$$

The atomic oxygen ions pass the electrolyte and are available for further reactions on the anode side. In general, the oxidation of hydrogen and carbon monoxide takes place. In fig. 2.4 this process is depicted. Depending on the efficiency of the reformer also methane is oxidized resulting in the following reactions:

$$H_2 + O^{2-} \rightarrow H_2O + 2e^- \tag{2.20a}$$
$$CO + O^{2-} \rightarrow CO_2 + 2e^- \tag{2.20b}$$
$$CH_4 + 4O^{2-} \rightarrow 2H_2O + CO_2 + 8e^- \tag{2.20c}$$

Using ionized atomic oxygen O^{2-} in the reactions gives a surplus of electrons in the products. These electrons are transported to the cathode side and used to ionize the oxygen.

Higher carbon-oxy-hydrates may get to the anode side of the stack if used in the fuel. It is not clear yet whether they are reformed in the reformer itself, leading to
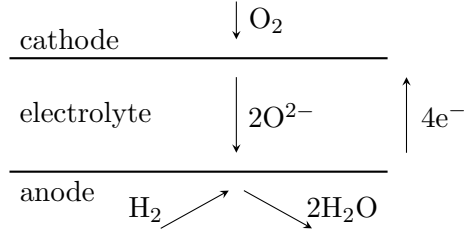
Figure 2.4: Schematic of the stack. Oxygen binds additional electrons on the cathode side and passes the electrolyte. On the anode side the fuel is oxidized and the additional electrons are released. In this figure H_2 is used as fuel. For other kinds of fuel, similar reactions occur. The electron transport from anode to cathode happens outside the cell. This is the resulting current.

the previously shown reactions, or oxidized directly [14]. Additionally to the change in the mass flow, the oxygen transfer also has an impact on the temperatures in the stack. On the anode side, the reaction enthalpy contributes to the total enthalpy of the anode gas. This change in enthalpy leads to a change in temperature.

2.5.2 Electrical properties

An electrochemical model can be derived from occurring reactions. This is realized by introducing the Nernst Potential U_N. The Nernst Potential is the theoretically highest possible potential for operating conditions. The Nernst Potential can be measured when no power is drained.

Most definitions of the Nernst Potential use the general Wagner Equation. It applies an integral and the chemical potentials at the anode and the cathode. This equation can be transformed into a more convenient notation. The exact derivation can be found in literature like [14]:

$$U_N = U_0 - \frac{RT}{zF} \sum_{i=1}^{N} \nu_i \ln \frac{x_i p_i}{p^0} \tag{2.21}$$

using the Faraday constant $F = N_A\, e = 96\,485.309\,\text{A} \cdot \text{s} \cdot \text{mol}^{-1}$, with the Avogadro constant N_A and the elementary charge e. z states the molar quantity of transferred electrons per reaction. The sum considers all species present in the reaction. For species i, ν_i denotes the molar quantity in the reaction, x_i the mole fraction and p_i the partial pressure. p^0 considers the absolute pressure. The first term on the right side is the standard potential U_0:

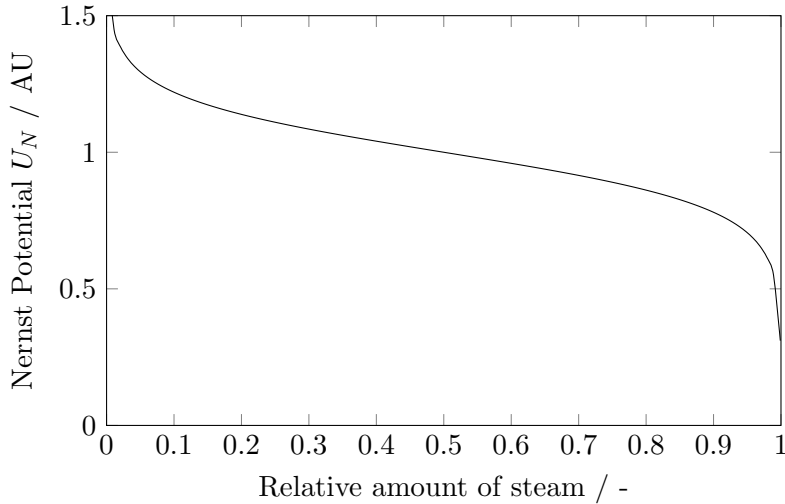$$U_0 = -\frac{\Delta_R G(T)}{zF} \tag{2.22}$$

28

Figure 2.5: Qualitative plot for the Nernst Potential over the relative amount of steam. Note the asymptotic pattern on both sides of the graph.

with the temperature depending Gibbs Enthalpy of the reaction $\Delta_R G(T)$. The naming of the standard potential can be misleading. It uses the standard pressure but not the standard temperature.

The calculation of the Nernst Potential contains a risk for the simulation in case of extreme values, due to the logarithm in (2.21). Especially in the case of lacking steam, the problem $U_N \to \infty$ occurs. This case implies a stack run with pure hydrogen and oxygen. At the moment of power drain, when measuring the potential, enough steam would be produced to reduce the Nernst Potential to a finite value. In figure 2.5, a qualitative plot for the Nernst Potential over the relative amount of steam can be seen. For most operation points, the losses in a cell can be modeled with an ohmic resistance. Solely close to the boundaries, nonlinear losses are prevalent. The ionic conductivity of the electrolyte has the most impact on the resistance. The resistances of anode and cathode are a few magnitudes smaller. Together they are responsible for the ohmic losses of the cell.

For low currents, activation losses appear. They are connected to the kinetics of the stack. Particularly the charge transfer is a limiting factor for the kinetics. It depends on the potential of the cell. In SOFCs, these losses are minor and negligibly compared to losses from leakage currents.

For high currents, concentration losses appear. Due to the high fuel conversion, the waste gas cannot be evacuated from the cell at a sufficient rate. This leads to the previously discussed problem for the Nernst Potential with high steam concentrations.

These losses are often joint to a total loss generated by an area specific resistance

ASR. The area specific resistance is a widely used property to describe the performance of a stack. It depends on the current and is given for a certain operation point [14]:

$$ASR = -\frac{dU(i)}{di} \tag{2.23}$$

To predict the area specific resistance all occurring and previously discussed resistances are summed and put in relation with the total cell area [15].

$$ASR = A_{cell} \sum_k R_k \tag{2.24}$$

From the electric properties also the efficiency η_{cell} of single cells and the stack can be deduced. Therefore the ratio of the measured potential U_{cell} and the ideal potential U_{ideal} is multiplied with the theoretically maximal efficiency η_{ideal}:

$$\eta_{cell} = \eta_{ideal} \frac{U_{cell}}{U_{ideal}} = 0.83 \frac{U_{cell}}{U_{ideal}} \tag{2.25}$$

The factor $\eta_{ideal} = 0.83$ comes from the efficiency of the reaction from pure hydrogen with pure oxygen at standard conditions ($T = 298.15\,\text{K}$, $p = 101\,325\,\text{Pa}$). The calculated efficiency η_{cell} is often referred to as voltage efficiency. For further considerations of the efficiency the fuel utilization can be used. Since the Nernst Potential is a function of the gas composition on both sides of the cell, it also depends on the fuel utilization. In case of a total fuel utilization the Nernst potential vanishes. Therefore, a residual amount of fuel is expected and also desired at the exit of the stack. [15]

2.6 Simulation Properties

For the simulation, some core properties have to be set. A constant sampling rate of $10\,\text{Hz}$ is chosen for the SIMULINK-model. This frequency matches the sampling rate of the experimentally collected data. Such a low sampling rate can be justified with the large thermal mass of the system. There are no expected thermal changes with a rate higher than $1\,\text{K} \cdot \text{s}^{-1}$. This value can be deduced from the data presented in [4]. At a common operating point of the order $1000\,\text{K}$, this corresponds to a relative change of $10^{-3}\,\text{s}^{-1}$.

Specific values for the simulation are preloaded during initialization. This includes external parameters like ambient temperature and ambient pressure, system-specific parameters like dimension and mass of a component, and general parameters like thermochemical data and other substance-specific features. Some of the substance-specific parameters depend on temperature and pressure. Therefore, interpolation tables are used. At the current point of the system development, those tables are only temperature-dependent. For the pressure, the standard condition of $p = 101\,325\,\text{Pa}$ is assumed. During the initialization also the initial conditions for each component are loaded.

2.6.1 Simulation Vector

The simulation uses different transfer parameters in addition to the component-specific input parameters. These transfer parameters comprise mass flow, temperature, and pressure. One of the goals of the simulation is to describe these three parameters at every point of the model. The sub-models of the components are used to vary these parameters.

The mass flow itself is modeled using a seventeen-dimensional vector. Each element $\dot{m}_i$ corresponds to the mass flow of the species i in $kg \cdot s^{-1}$. In table 2.1, the species used are listed. This vector is an expansion of the vectors used in previous models. For a more facile adaption of older systems and to avoid confusion, the order of the species corresponds to previous mass flow vectors. New species are appended to the previous vectors and kept in the same position for future adaptions. Carbon forms the sole exception. Carbon always occupies the last position on this vector. Pure carbon should form neither in the real system nor in the model. If this happens, carbon is usually deposited in the system. Therefore, it has no real propagation in the system in a gaseous state. It rather has to be observed on each component separately and incorporated in a carbon deposition model.

Table 2.1: The mass flow vector $\dot{m}_i$ used in the system with the corresponding species i. Carbon is missing in this vector since a propargation in the system is not expected. It has to be investigated in each component separately to detect depositions.

i	species	i	species	i	species
1	CO	7	N_2	13	$C_{12}H_{26}$
2	CO_2	8	Ar	14	C_8H_{18}
3	H_2O	9	C_3H_8	15	NH_3
4	H_2	10	C_4H_{10}	16	$C_{10}H_8$
5	CH_4	11	C_2H_6O	17	$C_{16}H_{34}$
6	O_2	12	CH_4O		

2.6.2 Thermochemical Data

Thermochemical data are required for the absolute evaluation of processes in the simulation. The simulation discussed in this work particularly needs values for the specific heat capacity at constant pressure c^p and the Gibbs Enthalpy G for all substances in the gas vector. The exact computation of these properties is too complex for dynamic simulation and cannot be implemented in real-time with the available resources. Therefore, tables are used.

Previous models are using the data provided in [16]. These data give values for numerous substances in 100 K steps. The data were taken from numerous publications and estimations. The tables often exceed the range 298.15 K to 1300 K. This range covers all known cases for the simulation. In the simulation, the tables are interpolated with a spline.

Gasteiger proposed in [17] to calculate those tables instead of manually entering them into the parameter files. This would make it possible to add new substances to the model by just adding a few values instead of a whole table. To calculate the properties, the empirical model proposed in [18] is used. The model uses seven coefficients to evaluate polynomials for specific heat capacity $c^p(T)$, enthalpy $H(T)$, and entropy $S(T)$ in the form of:

$$\frac{c^{p,0}(T)}{R} = \sum_{i=1}^{5} a_i T^{i-1} \tag{2.26a}$$

$$\frac{H^0(T)}{RT} = \frac{b_1}{T} + \sum_{i=1}^{5} a_i \frac{T^{i-1}}{i} \tag{2.26b}$$

$$\frac{S^0(T)}{R} = b_2 + a_1 \ln T + \sum_{i=2}^{5} a_i \frac{T^{i-1}}{i-1} \tag{2.26c}$$

with the gas constant R and gas specific coefficients a_i and b_i. The Gibbs Enthalpy $G(T)$ can be calculated using the relation:

$$G(T) = H(T) - S(T)T \tag{2.27}$$

For the temperature ranges 300 K to 1000 K respectively 1000 K to 5000 K two different sets of coefficients are used. Comparison with the data given in [16] shows a good correlation for $c^p(T)$ and $H(T)$ with a relative deviation below 5×10^{-2} and 10^{-1} respectively. $S(T)$ has a larger deviation from the literature values with an relative deviation up to 2×10^{-1}. For the relative deviation only values $T < 2300$ K are considered. The deviation for higher temperatures is larger in most cases, but those high temperatures can be omitted for contemporary fuel cell simulations. Furthermore, there is a discontinuity at 1000 K for many substances, giving a source for deviations. An extrapolation from the upper range (1000 K to 5000 K) down to 300 K could remove this discontinuity and can provide an even smaller relative deviation in some cases.

In [19], a subsequent publication to [18], a new polynomial approach with nine coefficients (instead of seven) is suggested. These polynomials also contain negative exponents in T:

$$\frac{c^{p,0}(T)}{R} = \sum_{i=1}^{7} a_i T^{i-3} \tag{2.28a}$$

$$\frac{H^0(T)}{RT} = \frac{b_1}{T} - a_1 T^{-2} + a_2 \ln T/T + \sum_{i=3}^{5} a_i \frac{T^{i-3}}{i-2} \qquad (2.28b)$$

$$\frac{S^0(T)}{R} = b_2 + a_3 \ln T + \sum_{i=1, i \neq 3}^{7} a_i \frac{T^{i-3}}{i-3} \qquad (2.28c)$$

The coefficients in (2.26) and (2.28) should not be confused with each other due to them having the same name. In the most cases, the nine coefficients polynomial gives a slightly smaller deviation for $c^p(T)$ and $H(T)$ in most cases. The magnitude of the deviation stays the same. It also removes the discontinuity at $S(1000\,\text{K})$ and reduces the relative deviation more than one magnitude to 5×10^{-3}. In fig. 2.6 some examples are shown for those deviations. In the examples the data for H_2O are chosen since it plays an important role during thermodynamic calculations. It seems that the deviation grows with the complexity of the molecule. For comparison the deviation of the entropy of C_8H_{18} is shown. There is only data for $T < 1000\,\text{K}$ since the molecule is not stable at higher temperatures. Compared to H_2O the deviation is increased by one magnitude.

It turns out calculating the thermochemical properties using the polynomials is not viable in the dynamic simulation. Therefore, the polynomials would be used only to generate an interpolation table before the simulation. This would result in a large deviation compared to the old tables, with the only benefit of making the model faster to extend. For the rest of this work, the data from [16] are used. This is done to make the results comparable to previous calculations of preceding projects. In the case of a deviation of measurements with the simulation results, using thermochemical properties from a different source may help to obtain more accurate results.

2.7 Previous Work

Soukup developed in the preceding work [4] a model of the cathode path of the system. In his work, the focus is put towards the burner, the heat exchanger, and the throttle valves. The model uses 14 different species in the gas vector.

The model of the burner uses the specific heat loss kA as a parameter. By variation of kA the model can be adapted without detailed knowledge of the geometry of the system. By variation of the thermic mass, the heating-up process can be modeled sufficiently and the model can be validated.

For the model of the heat exchanger, the parameters for specific heat transfer and specific heat loss can be varied. The model behaves like previous models and yields results sufficiently close to measured data when used with constant mass flows. With variable mass flows, too many variables enter the system, and it cannot be validated with the available data. The model of the heat exchanger is designed to fit the
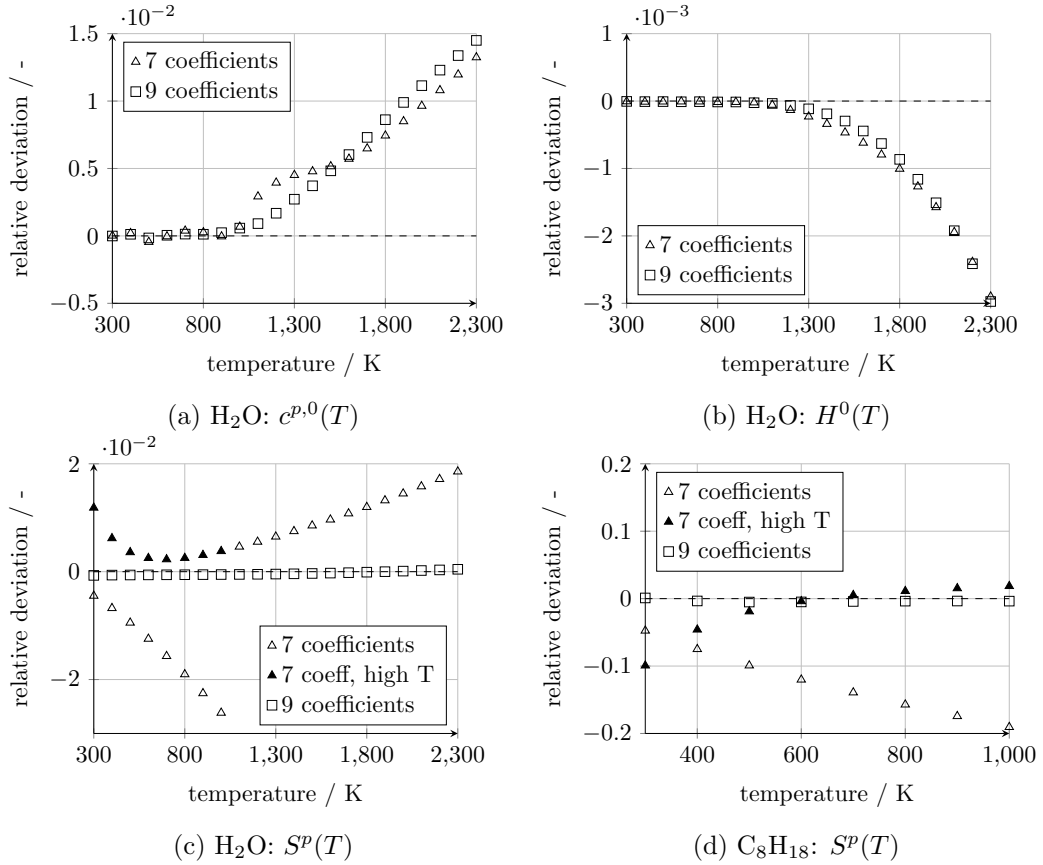
(a) H_2O: $c^{p,0}(T)$

(b) H_2O: $H^0(T)$

(c) H_2O: $S^p(T)$

(d) C_8H_{18}: $S^p(T)$

Figure 2.6: Examples for the temperature dependent deviation between thermo-chemical properties from different sources. The reference values are taken from [16]. The compared values are from seven coefficient and nine coefficient NASA polynomials from [18] (triangles) and [19] (squares). In the entropy plots the filled triangles come from the extrapolation of the high temperature data to low temperatures instead of using a different set of parameters. The subplots (a), (b), and (c) use data for H_2O. (d) shows only the deviation of the entropy for C_8H_{18}.

component in the cathode path. By calibrating a few parameters, this model should be viable for the heat exchanger in the anode path. With some further modifications, it should be possible to use it in the reformer and the stack.

To model the throttle valves, the theory of the isentropic nozzle flow is used. This model is also validated with measurements. The throttle valves in the system seem to behave differently. Especially at large aperture angles, the model yields no useful results. A second approach uses maps generated from measurements. Those maps still have problems with large aperture angles. The existing models are not suitable for the simulation and a better model has to be developed. For the next approach,

it is suggested to just vary the mass flow ratio between the two paths directly.

The temperature elements used appear to have a non-neglectable thermic mass. Therefore, the actual temperature may vary from the measured temperature. This makes it difficult to compare those data to the simulation. The simulated temperature could still be sufficiently close to the actual temperature, even though it does not fit the measurements. This effect may occur especially during fast temperature changes like during the heating-up process.

3 Simulation

This section deals with the implementation of the already discussed components in MATLAB and SIMULINK. To make the simulation real-time capable also some simplifications are considered and explained. For the simulation environment, a coarse version of the anode path is built. This path contains empty blocks for all desired modules to preserve the correct transfer of all variables. Between those blocks, the values are adjusted manually to ensure every block receives realistic input values. The sets of values are chosen accordingly to measured data for different operating points of the system. Subsequently, the fixed input values are substituted by the simulated output of each block and later used for comparison.

In this section, the data from several test series are used to calibrate the model. In the next section, the obtained calibration parameters are used to simulate the results for more data sets to predict the stability of the model. In case the parameters only need minor adjustments for different operating points, the model can be supposed as validated.

3.1 Reformer

3.1.1 Advanced Chemical Model

The classical approach in section 2.2.2 can give good results for simple systems. A system containing N different chemical compounds and using temperatures as an additional degree of freedom can be studied using an $N+1$-dimensional phase space. A system using only a system with three different gases ($N = 3$) would need a four-dimensional phase space. The simulations in this work are using $N = 17$ different gases. This would yield an equation system with 18 variables. Such a problem size should not be a problem using today's computing power. Still, this equation system could be simplified, e.g. by handling the temperature as a parameter. But the classical approach is difficult to formulate since most of the parameters are difficult to determine.

The temperature of the gas changes due to the reaction itself. These changes give a temperature gradient in the reformer [20, 21]. The reformer has fine geometrical features compared to its total size. These features make it difficult to describe the exact gas flow. Additionally, the precise composition of catalysts is usually unknown.

By determining these parameters, it would be possible to get the results for a few cases with a lot of effort.

For a dynamic model, these parameters have to be simplified. This simplification can be done by using a modified first-order kinetic model. This model makes it possible to use an effective temperature instead of a temperature gradient. The properties of the catalyst are combined with the geometry of the system and give a single rate constant.

For designing the kinetic model eq. (2.8) is considered. In the model, the reactions always use two reactants, therefore, a second-order approach ($n = 2$) should yield good results. Considering that some of the reactions are nearly unlimited in one reactant, $n = 1$ would be a better choice for some of them. Additionally, a catalyst is used for all reactions, which would demand $n = 0$. As a first guess $n = 1$ is used for the kinetic model, which uses exponential equations for the concentration in the form of (2.9).

Beginning with reforming of methane ($c = 1, h = 4, o = 0$), only the two equilibrium reactions (2.2) and (2.3) take place. The initial concentration $A_i(t_0)$ of each species is known. With these equations the second boundary value $A_i(t_\infty)$ can be determined. The first-order kinetic model is used to link those boundaries:

$$A_i(t) = A_i(t_0)e^{-kt} + A_i(t_\infty)(1 - e^{-kt}) \tag{3.1}$$

In this equation, k takes the place of a rate constant. The constant k should be a parameter depending on temperature since the Arrhenius equation asks for strong temperature dependence. The parameter k also depends on the reformer's geometry and the flow velocity. These two parameters can be linked to some sort of interaction time. A larger flow velocity would be equivalent to a smaller (shorter) reformer. The gas has less time to interact with the catalyst. Usually, the geometry is fixed and only the flow velocity can be regulated. In this work, k contains those design parameters implicitly if not stated otherwise. In figure 3.1 examples are given for different parameters k.

In the case of higher carbon-oxy-hydrates ($c > 1$), the cracking of those molecules has to be considered. Previous experiments have shown a lack of those higher carbon-oxy-hydrates in the reformed gas even though the equilibrium state has not been reached. This lack makes it possible to assume that this reaction has a high reaction rate and should be considered separately. The approach with the first-order kinetic model (3.1) is used again.
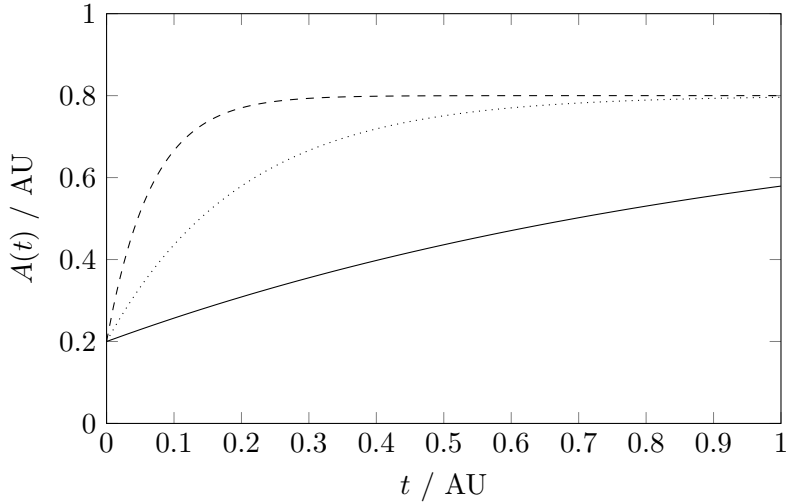
Figure 3.1: Examples for (3.1). The concentration $A_i(t)$ for a single i is plotted over time t, both in arbitrary units. All three curves use $A_i(t_0) = 0.2$ and $A_i(t_\infty) = 0.8$ with different values for k.
Dashed line: $k = 15$.
Dotted line: $k = 5$.
Solid line: $k = 1$.

To join these two reaction systems the resulting concentrations for the first set of reactions are named with $A_i(t)$ and for the second set $B_i(t)$. For both systems the equations using (3.1) are set up. To consider different reaction speeds, each equation gets its own k_j. By setting $B_i(t_0) = A_i(t)$ the two equations can be linked and they give the following set of equations:

$$A_i(t) = A_i(t_0)e^{-k_1 t} + A_i(t_\infty)(1 - e^{-k_1 t}) \tag{3.2a}$$

$$B_i(t) = A_i(t)e^{-k_2 t} + B_i(t_\infty)(1 - e^{-k_2 t}) \tag{3.2b}$$

For the evaluation of the parameters k_j only the product $k_j t_{int}$ is considered, using the interaction time t_{int} of the gas with the reformer. This step is also supported by the fact that there are only gas data available for the entrance ($t = t_0$) and the exit ($t = t_{end}$) of the reformer. This reduces the complexity of the system by one dimension. The equation system gives solutions for $k_j t_{int}$ when evaluated with gas data from experiments. There are only data available for $A_i(t_0)$ and $B_i(t_{end})$. This may result in a strong dependency of the $k_1 t_{int}$ and $k_2 t_{int}$ for data obtained in usual experiments.

The graph in figure 3.2 is not necessarily bijective. There can be multiple solutions for the interaction time for each output concentration $B_i(t)$. A unique solution requires more parameters of the system. For the system studied in this work, the
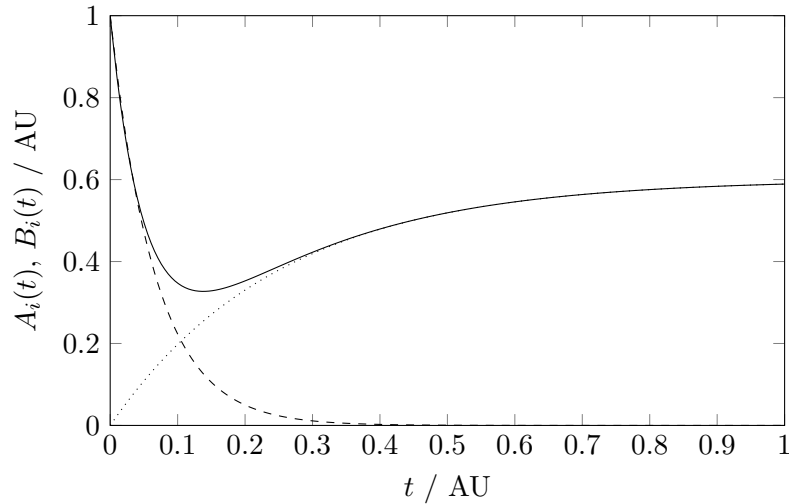
Figure 3.2: Example for the equations in (3.2). The concentrations $A_i(t)$ and $B_i(t)$ for a single i are plotted over time t, both in arbitrary units.
Dashed line: $A_i(t)$ with $A_i(t_0) = 1, A_i(t_\infty) = 0, k_1 = 15$.
Dotted line: $B_i(t)$ with $B_i(t) = 0, B_i(t_\infty) = 0.6, k_2 = 4$.
Solid line: $B_i(t)$ with $B_i(t) = A_i(t), B_i(t_\infty) = 0.6, k_2 = 4$.

temperature gradient was already measured by Fasching [21]. These measurements provide enough information for this system to determine a unique solution for the interaction time. From the interaction time, the rate constants can be deduced. The detailed application of this method is described in section 3.1.6.

3.1.2 Implementation of the model

In the next subsections, it is explained how the previously discussed chemical model is implemented in SIMULINK. Therefore the reformer is split into three submodules. First the *converter module* performs the cracking reaction (2.2) and reduces the complexity. The *equilibrium module* calculates the chemical equilibrium from the output vector of the converter module. In the last step, the *kinetic module* uses the original gas vector, the results from the converter module, and the results from the equilibrium module to compute the resulting gas vector. This process is depicted in figure 3.3.

Before and after the three main modules, auxiliary blocks are added. The blocks at both ends convert the units of the gas vector from a mass to an amount. This conversion is necessary because the modules in the reformer are simulating chemical reactions. The other auxiliary blocks are needed to adjust the length of the gas vector. As described in the next section, the gas vector is reduced in the converter module to five dimensions by mapping all reacting species onto the first five
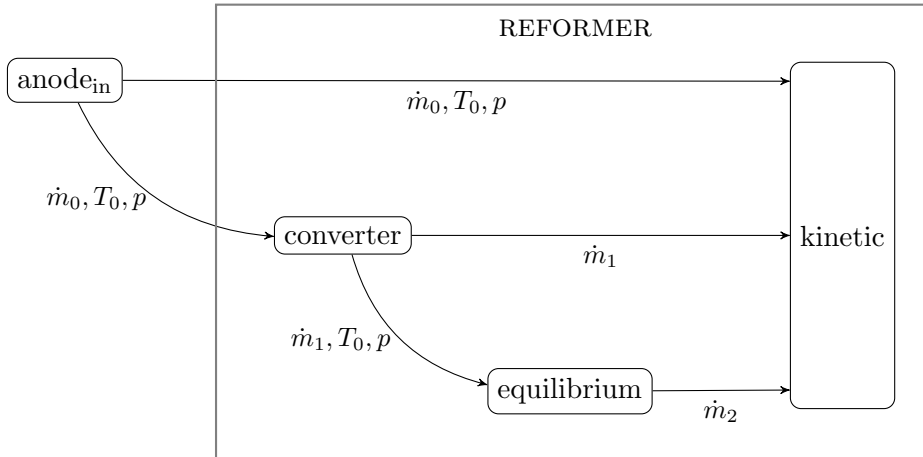
Figure 3.3: Implementation of the reformer. It is split into three submodules, each handling a different part of the chemical model:
converter module: performing the cracking reaction.
equilibrium module: calculates the chemical equilibrium via Gibbs minimization.
kinetic module: computes the resulting gas vector.

elements. The equilibrium module uses this five-dimensional vector for its computations. Before the kinetic module, both short gas vectors are expanded again to the full (seventeen dimensional) gas vector with zero padding. Non-reacting species bypass the converter and the equilibrium module. They are inserted into the gas vector before the kinetic module.

3.1.3 Converter Module

The converter reduces the complexity of the system for the equilibrium module. Every problem using different kinds of carbon-oxy-hydrates can be simplified to an equation system using only methane as fuel. This simplification corresponds to a transformation $\mathbb{R}^N \to \mathbb{R}^5$, with N describing the dimensions in the gas vector. This transformation is possible since the results of the equilibrium depend only on the sums of atoms and not the initial molecular composition. The benefits of a smaller system appear in an easier implementation, a faster evaluation, and a more predictable efficiency. In some ways, the converter module simulates the cracking of higher carbon-oxy-hydrates like in (2.2). In this work, the resulting gas vector is named the *reduced gas vector*.

First the total amounts c, o, and h of C, O, and H in the system are calculated from the initial gas vector. Evaluating the following equation system yields the reduced

gas vector:

$$co = \min[c, o] \tag{3.3a}$$

$$co_2 = 0 \tag{3.3b}$$

$$h_2o = \max[o - c, 0] \tag{3.3c}$$

$$h_2 = 0.5(h - 2\,h_2o - 4\,ch_4) \tag{3.3d}$$

$$ch_4 = \min[o - c, 0] \tag{3.3e}$$

A possible solution for this system may contain $h_2 < 0$, implying a negative amount of hydrogen in the reduced gas. Of course, this is not possible. It denotes a lack of H_2O in the initial gas vector. This case gives a warning in the simulation and should be avoided since it would lead to carbon deposition in a real system.

3.1.4 Equilibrium Module

The equilibrium module computes the most favored chemical composition of the gas. Its input parameters are the temperature and pressure for the wanted equilibrium, and the reduced gas vector. The module is built upon the static equilibrium module by Thaller [9].

The problem of using the static module in a dynamic simulation is not easily detectable. Changing only the temperature over time still gives reasonably accurate results. Changes in the composition of the gas vector are usually fatal. The static module uses the input values and compares them with the output values. Since a few time steps are needed to reach the equilibrium in a dynamic case, the module cannot complete its simulation. Still, the dynamic module uses the static module with some modifications.

The static module runs in an isolated box with its own clock. This box is implemented with a WHILE-loop. At every time step, the dynamic module calls the static module and waits for the equilibrium for a static case. The usage of a WHILE-loop involves some issues which have to be addressed. The WHILE-loop halts the global simulation until the equilibrium is reached. The number of iterations n affects the total simulation time in order $\mathcal{O}(n)$. To obtain reasonable simulation speeds a trade-off between speed and accuracy has to be made. For getting there a reasonable break condition has to be added. The upper limit is set by a maximum number of iterations. To prevent redundant operations a second break condition is added. There the relative change between two steps is investigated. Only gas values above a certain threshold are used for this break condition. Without this supplementary condition, small changes in quantities close to zero could cause problems. This threshold can be thought of as an AND-operation with the absolute change.

To compensate for the retardation of the overall simulation the complexity is reduced. The method has already been described in 3.1.3. The reduction to five

species promises to improve the performance since less complex equation systems have to be solved.

Tests show the equilibrium module is sensitive to changes in the total molar flow. Particularly the conservation of mass is affected. Further, the mass ratios are affected too. This problem is expected to result from the implementation in SIMULINK. To avoid this possible pitfall, the molar flow in this module is kept constant. This is allowed since the input and output gas vectors are linearly dependent. More specifically, the molar ratios can be decoupled from the absolute mass flow. Therefore a normalized gas vector is used. The normalization factor is used at the output of the module to obtain correctly scaled values. For the normalization, the most suitable molar flow can be determined over a series of tests and comparisons with gas data from the literature.

3.1.5 Kinetic Module

The third and final block in the reformer joins the results from the previous blocks and generates the final gas vector. Therefore the equations (3.2) are used. The three parameters $A_i(t_0)$, $A_i(t_\infty)$, and $B_i(t_\infty)$ are set by the initial gas vector, the converted gas vector, and the equilibrium gas vector.

For the exact determination of the rate constants k_j and the interaction time t_{int}, respectively the products $k_j t_{int}$, a separate evaluation of the model is needed, like proposed in section 3.1.1. This will be treated in the next section.

3.1.6 Gibbs Enthalpy

The enthalpy difference between the initial gas vector and the final gas vector can be used to change the temperature of the gas itself. This temperature change gives an additional boundary value for the rate constants of the kinetic module. Therefore, a closed system is assumed with no heat transfer between gas and reformer. This dependence of the temperature can be used to determine the parameters $k_j t_{int}$ of the kinetic module.

First, a reformer with infinite length is assumed. With a constant flow velocity, the interaction time translates into an interaction path. In this example, the gas composition would change over the length until it reaches the equilibrium state. In every point of this example, the enthalpy difference to the initial gas composition can be calculated. By converting this enthalpy difference into a temperature difference, a temperature profile for the system can be found. This profile can be compared with measured ones like the one by [21] (figure 3.4). To obtain a suitable parameter set $k_i t_{int}$, it is necessary to set some boundaries. First, the k_j are not considered as

independent variables. Instead it is possible to only use k_1 as variable and calculate k_2 using the factor a_k:

$$k_2 = k_2(k_1) = a_k k_1 \tag{3.4}$$

Since the first reaction (2.2) is considered fast in comparison to the other reactions, $a_k = 0.1$ is used as an initial condition. By varying the parameter a_k, a curve matching the measurements can be found. From this curve, it is possible to determine the length of the model, convert it into an interaction time, and finally obtain the parameters $k_i t_{int}$ for the system.
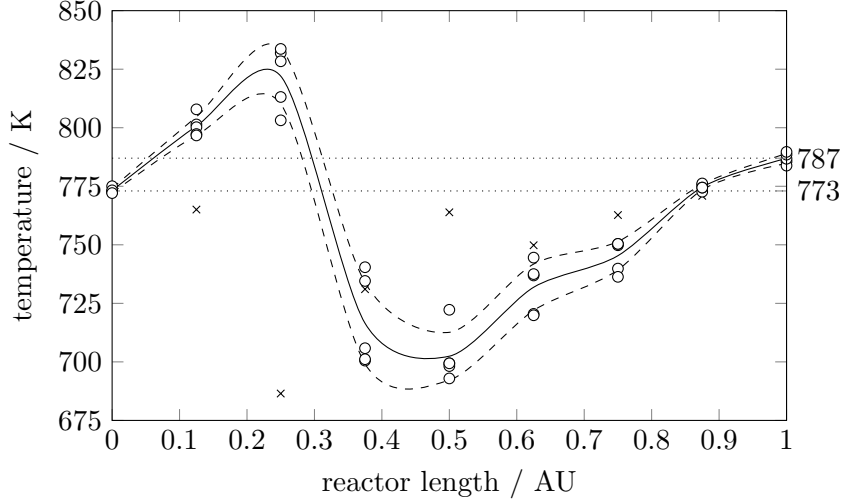

Figure 3.4: The temperature profile of the reactor used, as measured by [21]. The circles mark the measured temperatures at the different positions in the reactor. The solid line is an interpolated mean of those points with the standard deviation to both sides at the dashed lines. The measurement marked with crosses was omitted in that case, since it also has a strong divergence in the pressure loss (not shown) and probably resulted from a faulty setup. The dotted lines show the temperature difference $\Delta T = (14 \pm 3)$ K between the entrance and the exit of the reactor.

3.1.7 Heat balance

Until now, only the chemical aspects of the reformer have been discussed. The Gibbs enthalpy already gave a link to the thermodynamical side of the reformer. Further aspects are the heat capacity of the system and losses to the surroundings. The system used utilizes the waste heat of the cathode path to power the reformer. This is implemented with a heat exchanger containing the actual reformer. In the simulation, the model of the anode heat exchanger (section 2.7) is reused with different

parameters. For the heat balance, the reforming module is only completed with a heat exchanger module and a Gibbs enthalpy module, as shown in figure 3.5.

First, the reforming module computes the final gas vector. The Gibbs module uses this new vector and computes the enthalpy difference to the old one. The heat exchanger then uses the final gas vector and the input temperature for the anode path. The output of the Gibbs module is used like an additional heat source or heat drain in the anode path.

The output temperature in the anode path is used as the input temperature for the reforming module. Tests have shown that the equilibrium using the output temperature gives good results. A delay is inserted, to boost the performance of the model. To ensure the right temperature is used, the step size of the system has to be small compared to appearing dynamics. It has to be emphasized, that the chemical equilibrium is calculated with the temperature of the previous time step. This delay should not cause problems in the overall error due to the assumptions made in section 2.6.

This setup yields acceptable results for semi-stationary and low dynamic cases. For a better response in more dynamic systems, splitting the reformer into more segments can improve the accuracy. In a system without heat recovery, the heat exchanger module can be replaced by a module that only considers the enthalpy difference for the temperature change of the gas.

3.2 Junction

In a Junction two or more gasses are united and a mixing temperature is calculated. The resulting gas vector is obtained by an addition. For the mixing temperature the total caloric energy of the gas is calculated. With the heat capacity of the gas the new temperature can be calculated with (2.18). To avoid the integral in the simulation an iterative approach using (2.17) is chosen. (2.17) can be written with different indices as:

$$T_{mix,n+1} = \frac{\sum_i \dot{Q}_i}{\sum_j \dot{m}_j c_j^p(T_{mix,n})} \tag{3.5}$$

As a starting point $T_{mix,0}$ any temperature can be chosen. In SIMULINK a WHILE-block is used. This gives the possibility to obtain a very accurate temperature for every time step. The break condition for the loop is

$$|T_{mix,n+1} - T_{mix,n}| < T_{error} \tag{3.6}$$

whereas T_{error} denotes the absolute error. For this work $T_{error} = 0.5 \, \text{K}$ provides a sufficient accuracy combined with a reasonable simulation time. It can be compared
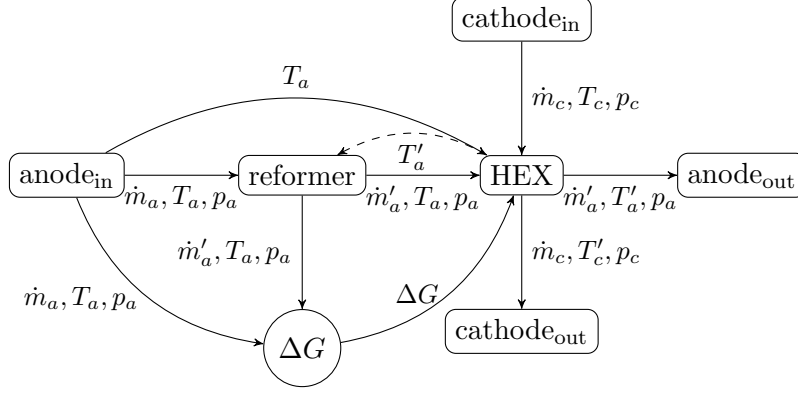
Figure 3.5: Flow chart of the enhanced reformer: Thermodynamical behaviour is added to the anode path, as well as thermodynamical coupling of the anode path and the cathode path. The subscripts a and c are to distinguish between anode and cathode path.
reformer: chemical part of the reformer presented in fig. 3.3.
HEX: Heat exchanger.
ΔG: difference in the Gibbs enthalpy is considered in *HEX*.
The dashed arrow T_a' from *HEX* to *reformer* forwards the resulting temperature of the previous time step. This temperature is used for the chemical reactions in the reformer.

to a relative error of order 10^{-3}. To improve the performance of the model better guesses for $T_{mix,0}$ can be used. A good guess for the mixing temperature is the mixing temperature of the previous time step $T_{mix,0}(t) = T_{mix}(t-1)$. Still for the first time step of the simulation a manual value has to be chosen. Using the ambiance temperature $T_{mix,0}(t=0) = T_{amb}$ gives the best results for this work.

3.3 Evaporator

The evaporator is used to insert liquid fuels into the system. The thermic energy of the recycled gas is used to evaporate the liquid fuel. The junction model is modified to include the heat of vaporization. Therefore in (3.5) the heat of vaporization Q_{vap} is subtracted from the total heat. Due to the special geometry of the system the evaporator receives additional heat from surrounding components. This heat flow is combined in $\dot{Q}_{ext}$ leading to the final equations for the evaporator temperature:

$$T_{mix,n+1} = \frac{-\dot{Q}_{vap} + \dot{Q}_{ext} + \sum\limits_{i} \dot{Q}_i}{\sum\limits_{j} \dot{m}_j c_j^p (T_{mix,n})} \tag{3.7}$$

46

In this version of the simulation, the heat flow $\dot{Q}_{ext}$ is implemented with a constant value. This value is changed according to the operation mode of the system.

3.4 Venturi

The mass flow in the anode path can be measured indirectly with the Venturi tube. The simulation uses these data to adjust its mass flow to match the measurements. The adjustment is handled by setting the recycling rate for the anode path to a suitable value. The main problem is the location of the evaporator. It is built in between the manifold and the Venturi tube. Therefore, the mass flow in the Venturi tube consists of the evaporated gas and an adjustable amount of recycled gas.

The Venturi equation for the mass flow (2.14) depends on the density of the gas. The density is unknown at the time of evaluating this expression, but can be calculated using the mass flow. This dependence makes this problem self-referential and requires an iterative solution. In figure 3.6 the flowchart for this process is depicted.

In the first step, the manifold module recycles 70 % of the incoming mass flow. This gas vector is lead through the evaporator module. The gas vector with added fuel is evaluated in the Venturi module. The Venturi module sends the demanded total mass flow back to the manifold. On the way back the total mass added by the evaporator module is subtracted, leaving only the mass needed from the manifold. Then the manifold module starts the next iteration with an improved recycling rate.

In the first attempts, this iteration cycle was put into a WHILE-loop to ensure accurate mass flow. It showed that the recycling rate only has low dynamics. This lead to the decision to remove the loop and sent the demanded value back with a delay. The delay improves the performance of the system. The only problem may be a larger deviation in the first few steps when starting the simulation.
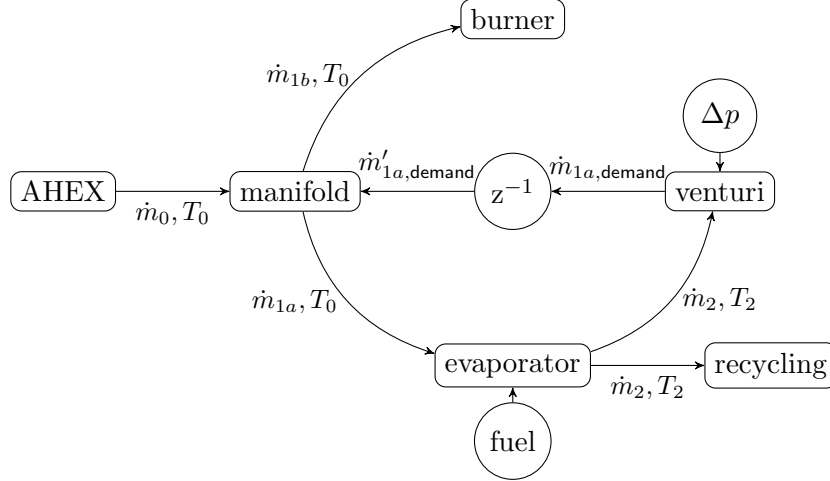
Figure 3.6: Flow chart for the stepwise manifold-venturi-system. In the first n-th step the manifold splits the massflow $\dot{m}_0$ into $\dot{m}_{1a}$ and $\dot{m}_{1b}$ according to the information $\dot{m}'_{1a,\text{demand}}$. $\dot{m}_{1a}$ passes the evaporator and fuel is added. The resulting $\dot{m}_2$ and T_2 are forwarded to the venturi nozzle. With the the pressure difference Δp the demanded massflow $\dot{m}_{1a,\text{demand}}$ is calculated. $\dot{m}_{1a,\text{demand}}$ is used in the $(n+1)$-th step to control the manifold.

3.5 Stack

The stack is the second link between the anode path and the cathode path. Additionally to the heat transfer also a mass transfer takes place. The model uses a coarse one-dimensional model consisting of two points, one at the entrance of the stack and one at the exit. In the calculation of the Nernst Potential U_N, a zero-dimensional model can lead to large inaccuracies and possible discontinuities. Therefore, the one-dimensional approach is favored.

The model uses the stack current in addition to the gas vectors, the temperatures and the pressures of the anode path and the cathode path. The molar oxygen transfer $\dot{n}_{O_2}$ from cathode to anode can be calculated using the current I.

$$\dot{n}_{O_2}(I) = \frac{I}{zN_Ae} = \frac{I}{4F} \tag{3.8}$$

Here $z = 4$ since every O_2 molecule contributes 4 electrons to the current. The calculated amount of O_2 is then subtracted from the gas vector of the cathode side and added to the gas vector on the anode side.

To calculate the resulting gas vector for the anode path the equilibrium model is used again instead of evaluating the stack reactions (2.20). This approach also avoids the uncertainty as to whether remaining higher carbon-oxy-hydrates are reformed

or directly oxidized. A copy of the reformer block is inserted into the stack block with some modifications. First, the kinetics of the reactions are neglected since the gas remains relatively long in the stack. Therefore, only the converter module and the equilibrium module are kept. The thermodynamic components of the reformer are also omitted here and combined with further calculations, as described later in this section. Thus, only the chemical equilibrium is used for the resulting gas vector. The temperature used for the equilibrium is taken from the output of the stack from the previous time step. The calculation of that temperature is explained later in this section. A simplified flow chart is shown in fig. 3.7.

For the calculation of the Nernst Potential, the arithmetic average of the input and output gas vector is used. This average helps to prevent unrealistic high and low values that could occur due to the logarithm in (2.21). This method may work since the equation for the Nernst Potential can be fitted with a linear function for a wide span. For a more precise prediction of the Nernst Potential a more-dimensional model of the stack is needed.
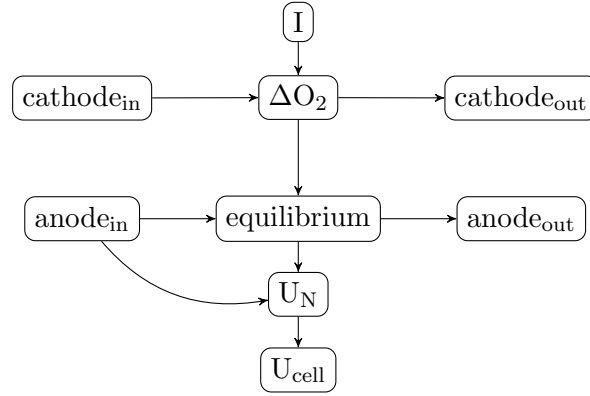

Figure 3.7: Simplified flow chart for the stack: With current I a transfered amount of O_2 is caluclated. This amount is added to the anode path with an equilibrium module. The Nernst Potential U_N is calculated before and after the transfer and averaged. From there the cell voltage U_{cell} is calculated.
The thermodynamical coupling of the anode and the cathode path is not shown. This could be realized like shown in fig. 3.5.

To calculate the potential of a cell U_{cell} a source with an internal resistance is assumed. The circuit for the model is shown in figure 3.8. The Nernst Potential is used as a basis. Then an ohmic loss U_{loss} is subtracted. The ohmic loss is calculated with the taken current I and the given (datasheet from the cell manufacturer) area specific resistance ASR over the area of a single cell:

$$U_{cell} = U_N - U_{loss} = U_N - I\frac{ASR}{A_{cell}} \tag{3.9}$$

To get the total potential of the system U_{stack} the potential of a single cell is multiplied with the number of cells in the system N:

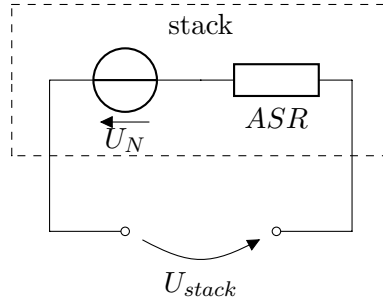$$U_{stack} = NU_{cell} = U_N - I\frac{ASR}{A_{cell}} \tag{3.10}$$

Figure 3.8: Circuit for the calculation of the total potential of the system U_{stack}, using the Nernst Potential U_N and the area specific resistance ASR.

For the heat balance, the corresponding segments from the reformer block are copied. Again the Gibbs module computes the enthalpy differences between input and output gas vector. The heat exchanger then uses an additional heat source input for each side of the stack. On the cathode side, the stored heat of the transferred oxygen is added. The anode side uses the output of the Gibbs module like in the reformer. The electric energy losses due to cell resistance also contribute to the heat balance. In the model, they are divided equally to both sides.

Like for the reformer this setup yields acceptable results for semi-stationary and low dynamic cases. Splitting the stack into smaller parts can improve accuracy. When using smaller segments, the effect of the reaction kinetic has to be investigated and should be considered.

4 Results and Discussion

In this section, the validation of the models from section 3 is discussed. The already discussed calibration has been done with the major part of available data sets. Other untouched data sets are used for the validation. This way the validation yields relatively objective results and provides a better basis for improvements. First, the results for the reformer are presented and discussed. Later, results for the whole system are provided.

4.1 Evaluation of the Reformer

For the validation of the reformer, two aspects have to be discussed separately. First, the equilibrium reactor is discussed, and second, the complete reforming module. The results of the equilibrium module are compared with literature values. The reforming module is calibrated and validated with data generated by the proposed system.

4.1.1 Validation of the equilibrium module

For the validation of the equilibrium module, the literature data [6] are taken as a reference. The data are from a heated steam reforming test. The tests have been conducted with diesel and steam at $SCR = 1.5$. In the simulation, the input-gas-vector was constructed differently. The gas composition at three different temperatures $T = \{573, 973, 1373\}$ K in the dataset is evaluated. From these three vectors, the corresponding elemental ratios are calculated and then averaged. The converter module generated a new gas vector. This conversion is valid since the equilibrium only depends on the molar ratio of each element rather than each species. The comparison of the molar concentrations is shown in fig. 4.1.

The comparison of simulated equilibrium data with this test is possible since in [6] the reaching of the equilibrium is expected. In the simulation, a carbon deposition rate of 0.85 is used since it showed to generate the best results. The soot concentration shows a large error of up to 50%. An advanced approach is needed to solve this problem. At higher temperatures, this problem does not occur since no carbon
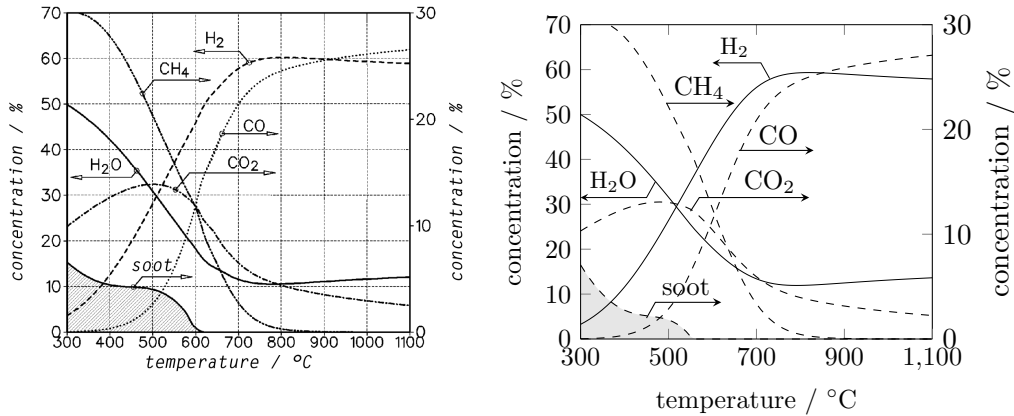
Figure 4.1: Comparison of data from literature [6] (left) with data obtained with the equilibrium module implemented in SIMULINK (right). The simulated values with solid line use the left axis, the ones with the dashed line the right axis.

deposition takes place. For the other species, the equilibrium module generates qualitatively similar results to the experimental data. The module is a simple approach to estimate the gas composition of reforming reactions.

The evaluation of the literature data at different temperatures is necessary since the elemental ratio is not constant for all temperatures. This error may come from the experimental setup. For the comparison with the simulation, one could use the gas-vector for each temperature value to simulate the corresponding equilibrium concentration. In this case, the average from three different temperature steps is sufficient to show the qualitative functionality of the equilibrium module. For quantitative analysis, more reliable data are needed.

4.1.2 Validation with gas measurements

The functionality of the equilibrium module has been shown in the last section. In this second step of the reformer validation, the kinetic module is added, and therefore the whole reformer is investigated. Exemplarily it is attempted to reproduce experimental data from two different tests with the reformer model. The measurements provide consecutive data for more than one hour each. Primarily the two tests differ in the fuel used. One was performed using natural gas (CH_4), the other using diesel. Here again, only gas data are compared.

The gas measurements have been performed on dry gas. Steam was separated before the measurement. Therefore, H_2O does not occur in the experimental data. Furthermore, only species with a concentration $> 10^{-3}$ are investigated. The gas vector reduces to the four dimensions {CO, CO_2, H_2, CH_4}. The resulting gas vector from

the simulation is transformed into the same form by omitting H_2O and all other species with concentrations $< 10^{-3}$. The vectors are normalized afterward. The comparison for the test using natural gas is shown in fig. 4.2, the test using diesel in fig. 4.3.
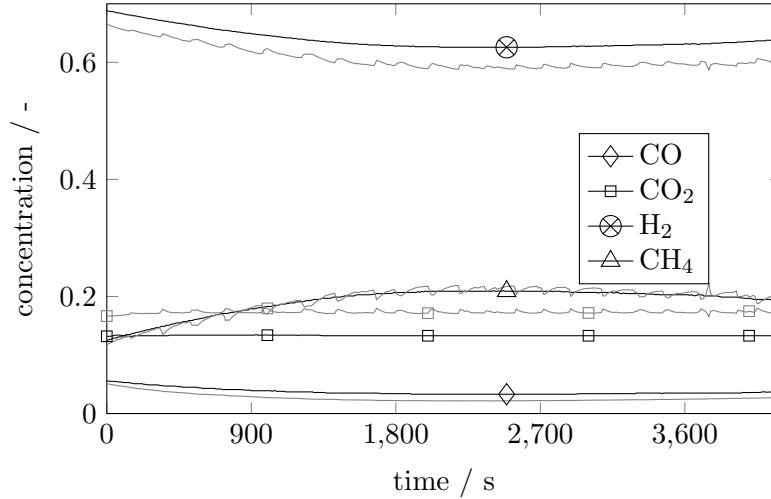

Figure 4.2: Comparison of dry gas measurements with simulated data. The fuel used in the test was CH_4. The black lines are generated with the experimental data. The corresponding gray lines are the simulated reproduction of the black lines.

For the test using CH_4, the concentrations for CO and CH_4 can be replicated well. The simulated concentrations for CO_2 and H_2 show overall fitting behavior but exhibit a quite large offset to the measured data. The simulated concentration for H_2 is strictly lower than the measured one. Therefore, an error due to a higher theoretical efficiency can be excluded.

Overall the comparison in the case of diesel gives similar results as with CH_4. Again, an offset can be observed for the concentrations of CO_2 and H_2.

Acknowledging the functionality of the equilibrium module, the deviation between measured and simulated data may result from the kinetic module. The temperature has a huge impact on the kinetic, as already stated. In the current model, the temperature only affects the equilibrium but not the kinetic itself. For future approaches, the kinetic model may be expanded by a temperature dependency.

4.2 Evaluation of the Recycling

Another scrutinized mode of the system is the *rate of recycling*. As mentioned earlier, the rate of recycling is inevitable for obtaining correct values for the gas
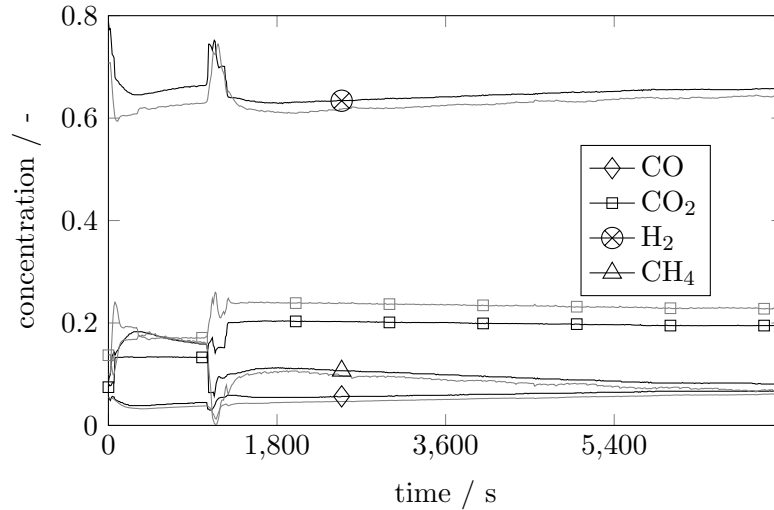
Figure 4.3: Comparison of dry gas measurements with simulated data. The fuel used in the test was diesel. The black lines are generated with the experimental data. The corresponding gray lines are the simulated reproduction of the black lines.

vector. Here, data for the rate of recycling are presented for a case without load. A test case in which diesel was utilized as fuel is used. The time window of the test case is right after the heat up of the system. Only changing parameters are fluctuations in the input mass flows.

In figure 4.4 the rate of recycling is depicted. During the $2000\,s$ of the test case, the rate of recycling stays between $0.960 < rate\ of\ recycling < 0.970$. Overall, the rate of recycling shows an upwards trend with positive curvature. On a smaller time scale, noise can be observed with some distortions.

The simulation seems to be stable. The trend on the large timescale may have two possible reasons. First, the equilibrium state of the system has not been reached yet. Second, the microenvironmental conditions may have slightly changed during the test. Even though the laboratory conditions have been constant during the test, small heat domains could have formed in the system, undetected by the laboratory sensors. Important to note the simulation does not take into account the surroundings of each component but only the laboratory conditions.

The noise on smaller timescales may result from the input data also containing noise. The main sources are to be assumed to be the air blower and the evaporator. The noise also indicates a fast response of the recycling module to changes in the input.
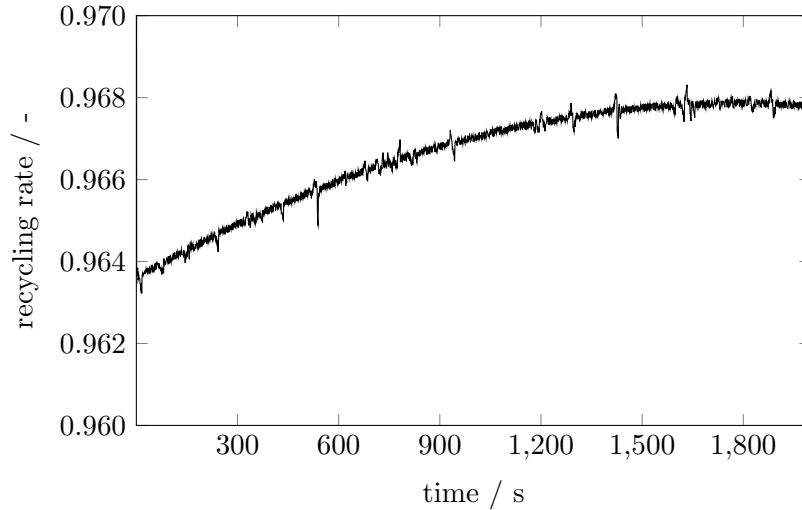
54

Figure 4.4: Simulated rate of recycling over time with data from a test case utilizing diesel as fuel. The test case is without external load.

4.3 General Remarks

We already discussed the simulation results of the reformer and the recycling. There are some deviations that cannot be explained by just tweaking the model parameters. Those deviations may be the result of some missing energy transports in our model, as mentioned in 2.1.7. We ignored those heat transfers for this model due to their complexity, on one hand, on the other hand, the basic model was intended to not depend on the current geometry of the system. Future approaches could take this heat transfer into account to some extend, by investigating the temperature difference of neighboring components. By only implementing the groups with the largest difference in temperature, the overall accuracy of the model could be improved with reasonable effort.

5 Conclusion and Outlook

SOFC systems can convert chemical energy to electrical energy efficiently. In comparison to a basic fuel cell, the metal-based membrane allows higher operation temperatures. The high temperatures make expensive catalysts obsolete and allow to power the cell with a variety of different fuels. An existing SOFC system, located at AVL Graz, Austria, was investigated in this work. A partially existing simulation model was expanded and improved. These improvements can be split into three topics.

First, chemical reactions in the reforming process have been scrutinized. The dominant reactions were the cracking of higher carbon-oxy-hydrates with steam, its reversible for methane, and the reversible water-gas-shift. To take the kinetics into account, the pre-reformer model applies a simplified version of the cracking reaction to the gas stream. Then the equilibrium is computed using a Gibbs minimization method. The pre-reformer model was trained with data from gas measurements and later evaluated. The model could predict the resulting gas vector qualitatively for tests using CH_4 and diesel as fuels. Still, systematic deviations occur in all runs.

Second, fuel recycling was added to the simulation. A part of the partially burned fuel is re-used. Recycling helps to obtain higher efficiencies, lower emissions, and higher stability of the system due to the larger gas-stream. The simulation uses data from the built-in venturi tube to compute the recycling rate. An iterative algorithm is used. To have a fast real-time model, this algorithm is not executed in each timestep. Instead, at every timestep, only one iteration is made. For a stable simulation, an initial guess is sufficient.

Third, the literature data of thermodynamical values are compared to each other. The previous simulation models used tables containing values from [16] or a polynomial approach proposed in [18]. The data points of the investigated molecules are diverging at higher temperatures. For small molecules like H_2O, the relative difference was around 10^{-2} at $1000\,\mathrm{K}$. For larger carbon-oxy-hydrates, the relative difference was examined at about 10^{-1} for all temperatures found in the SOFC system. A second issue is the inconsistency of the polynomials from [18] at $1000\,\mathrm{K}$. The improved polynomials proposed in [19] could solve both above-mentioned problems.

This work improved the partially existing model but also opened the door to some future research. Three major topics need some future consideration:

1. The kinetics model still needs improvement. An implementation of a temperature dependency may help.

2. The noise in the recycling model is not understood completely. Correlating speed data from the compressors to the simulation results could be a starting point for a better understanding.

3. Heat transfers in the current model are coupled to the gas flow and the heat exchangers. There may be further heat transfers which can be only found by investigating the physical system.

Bibliography

[1] Shobit Omar et al. "Ionic Conductivity of Plasma-Sprayed Nanocrystalline Yttria-Stabilized Zirconia Electrolyte for Solid Oxide Fuel Cells." In: *Scripta Materialia* (June 2009), pp. 1023–1026. DOI: `10.1016/j.scriptamat.2009.02.036`.

[2] Subhash C. Singhal and Kevin Kendall. "Chapter 1 - Introduction to SOFCs." In: *High Temperature and Solid Oxide Fuel Cells*. Ed. by Subhash C Singhal and Kevin Kendall. Amsterdam: Elsevier Science, 2003, pp. 1–22. ISBN: 978-1-85617-387-2. DOI: `10.1016/B978-185617387-2/50018-0`.

[3] Marian Forster. "Modelbased Control Design of High Temperature Fuel Cells." MA thesis. University of Technology Graz, Institut für Regelungs- und Automatisierungstechnik, 2018.

[4] Nikolaus Soukup. "Dynamische Simulation eines stationären SOFC-Systems." MA thesis. Technische Universität Graz, Institut für Wärmetechnik, 2017.

[5] R. Mark Ormerod. "Chapter 12 - Fuels and Fuel Processing." In: *High Temperature and Solid Oxide Fuel Cells*. Ed. by Subhash C Singhal and Kevin Kendall. Amsterdam: Elsevier Science, 2003, pp. 333–361. ISBN: 978-1-85617-387-2. DOI: `https://doi.org/10.1016/B978-185617387-2/50029-5`.

[6] Stephan Montel. "Brenngaserzeugung aus Dieselkraftstoff für den Einsatz in Brennstoffzellenantrieben." PhD thesis. Forschungszentrum Jülich, Institut für Werkstoffe und Verfahren der Energietechnik, 2003.

[7] Juliana Piña and Daniel Borio. "Modeling an Simulation of an Autothermal Reformer." In: *Latin American applied research* 36 (Oct. 2006), pp. 289–294.

[8] Mark W. Smith and Dushyant Shekhawat. "Chapter 5 - Catalytic Partial Oxidation." In: *Fuel Cells: Technologies for Fuel Processing*. Ed. by Dushyant Shekhawat, James J. Spivey, and David A. Berry. Amsterdam: Elsevier, 2011, pp. 73–128. ISBN: 978-0-444-53563-4. DOI: `https://doi.org/10.1016/B978-0-444-53563-4.10005-7`.

[9] Yvonne Thaller. "Dynamische Modellierung eines SOFC-Stacks und Reformers." MA thesis. Campus 02, Graz, 2016.

[10] P. Atkins and J. de Paula. *Atkins' Physical Chemistry*. OUP Oxford, 2010. ISBN: 9780199543373.

[11] J. Larminie and A. Dicks. *Fuel Cell Systems Explained*. J. Wiley, 2003. ISBN: 9780768012590.

[12] S. Gordon et al. *Computer Program for Calculation of Complex Chemical Equilibrium Compositions and Applications. I. Analysis.* NASA reference publication. National Aeronautics, Space Administration, Office of Management, Scientific, and Technical Information Program, 1994.

[13] C.E. Mortimer. *Chemistry.* Wadsworth series in chemistry. Wadsworth Pub. Co., 1983. ISBN: 9780534011840.

[14] M. Bieber. "Messmethoden zur Untersuchung der Kohlenstoffablagerung an nickelhaltigen SOFC-Anoden beim Betrieb mit Methan." PhD thesis. Technische Universität München, Fakultät für Maschinenwesen, 2010.

[15] Inc. EG& Technical Services. *Fuel Cell Handbook (Fourth Edition).* U.S. Department of Energy, 2004.

[16] Ihsan Barin and Gregor Platzki. *Thermochemical Data of Pure Substances.* VCH, 1995.

[17] Marika Gasteiger. "Prozesssimulation einer NH3-SOFC-Anlage." MA thesis. Technische Universität Graz, Institut für Wärmetechnik, 2018.

[18] Bonnie J. McBride, Sanford Gordon, and Martin A. Reno. *Coefficients for Calculating Thermodynamic and Transport Properties of Individual Species.* Technical Memorandum 4513. NASA, Nov. 1993.

[19] Bonnie J. McBride, Michael J. Zehe, and Sanford Gordon. *NASA Glenn Coefficients for Calculating Thermodynamic Properties of Individual Species.* Technical Publication 2002-211556. NASA, Oct. 2002.

[20] Huisheng Zhang, Shilie Weng, and Ming Su. "Compact Heat Exchange Reformer Used for High Temperature Fuel Cell Systems." In: *Journal of Power Sources* 183 (Mar. 2012). DOI: 10.1016/j.jpowsour.2008.04.068.

[21] Karin Fasching. "Untersuchung zu Diesel-Steam-Reforming für SOFC-Systeme." MA thesis. Technische Universität Wien, 2015.